Nuclear Instruments and Methods in Physics Research A 803 (2015) 68–81

Contents lists available at ScienceDirect

Nuclear Instruments and Methods in Physics Research A

journal homepage: www.elsevier.com/locate/nima

A portable and wide energy range semiconductor-based neutron spectrometer

C.B. Hoshor [a], T.M. Oakes [b], E.R. Myers [a], B.J. Rogers [a], J.E. Currie [a], S.M. Young [a], J.A. Crow [a], P.R. Scott [a], W.H. Miller [b,c], S.L. Bellinger [d], T.J. Sobering [e], R.G. Fronk [d], J.K. Shultis [d], D.S. McGregor [d], A.N. Caruso [a,*]

[a] Department of Physics, University of Missouri, Kansas City, MO, United States
[b] Nuclear Science and Engineering Institute, University of Missouri, Columbia, MO, United States
[c] Missouri University Research Reactor, Columbia, MO, United States
[d] Department of Mechanical and Nuclear Engineering, Kansas State University, Manhattan, KS, United States
[e] Electronics Design Laboratory, Kansas State University, Manhattan, KS, United States

ARTICLE INFO

Article history:
Received 31 July 2015
Received in revised form
27 August 2015
Accepted 28 August 2015
Available online 24 September 2015

Keywords:
Neutron spectrometer
Solid-state neutron detector
Neutron source identification
Portable neutron detector
Moderating spectrometer
Semiconductor-based neutron detector

ABSTRACT

Hand-held instruments that can be used to passively detect and identify sources of neutron radiation—either bare or obscured by neutron moderating and/or absorbing material(s)—in real time are of interest in a variety of nuclear non-proliferation and health physics applications. Such an instrument must provide a means to high intrinsic detection efficiency and energy-sensitive measurements of free neutron fields, for neutrons ranging from thermal energies to the top end of the evaporation spectrum. To address and overcome the challenges inherent to the aforementioned applications, four solid-state moderating-type neutron spectrometers of varying cost, weight, and complexity have been designed, fabricated, and tested. The motivation of this work is to introduce these novel human-portable instruments by discussing the fundamental theory of their operation, investigating and analyzing the principal considerations for optimal instrument design, and evaluating the capability of each of the four fabricated spectrometers to meet the application needs.

1. Introduction

Portable instruments that can detect and identify neutron sources by high intrinsic efficiency and energy-sensitive measurement of free neutrons, ranging from thermal energies (<0.025 meV) to top end of the evaporation spectrum ($\sim$20 MeV), are important to applications in non-proliferation and health physics. For non-proliferation applications, the goal is a sensitivity and spectroscopic resolution that will allow for unknown source detection and identification from neutrons alone as a crude complement to portable gamma-ray spectroscopic instruments; detection over the large energy range is important for sources in unknown moderating/absorbing configurations. In health physics applications, the neutron dose equivalent rises and falls more than two-orders of magnitude between the thermal and 14-MeV energy range, presenting substantial dosimetry challenges. In commercially available rem meters [1] the average dose equivalent error is significant due to poor energy sensitivity in the upper end of this large range. To address the challenges inherent to these applications, this work presents and compares the empirical and computational design and results of a new class of real-time human-portable neutron spectrometer, building from the foundation established by Bonner [2], and enabled by the high thermal neutron detection efficiency density (thermal neutron detection efficiency per unit active volume) and spatial resolution of semiconductor-based neutron detectors [3].

2. Instrument design

2.1. Background

The instrument geometries, detector-moderator configurations, analysis methods, and results described here are synthesis of, and improvement on, the multi-sphere- and long-counter-based moderating-type neutron spectrometers [2,4]. The major deficiencies in the multi-sphere spectrometers are: (a) the inability to measure neutron intensity with each sphere radius simultaneously, (b) the poor spatial resolution of detected thermalized neutrons, (c) the very low intrinsic neutron detection efficiency, and (d) the unportable mass of the near largest to largest radius moderating

* Correspondence to: 257 Flarsheim Hall, 5110 Rockhill Road, Kansas City, MO 64110, 816-235-2505.
E-mail address: carusoan@umkc.edu (A.N. Caruso).

http://dx.doi.org/10.1016/j.nima.2015.08.077
0168-9002/

sphere used to measure neutron intensity at the top end of the fast neutron energy range (i.e., a 30-cm radius). In the long counter design, neutron intensity is measured axially in a cylindrical geometry, replacing the radial dependence of the measured neutron intensity in the spherical geometry. Although the cylindrical geometry prevents equal sensitivity over 4π, an instrument with a portable mass that can still provide enough low-Z cross-section to thermalize a 14-MeV neutron is gained. The downfall of the single position-sensitive sensor in the long counter design is its low intrinsic efficiency and crude energy resolution, even in advanced designs [5,6]. While adding axial sensors radially can theoretically improve the intrinsic efficiency as well as the energy and spatial resolution of a long-counter, a large fraction of the moderating medium must be displaced, increasing both the volume and overall instrument mass [7]. What is needed is a different type of thermal neutron sensor that yields minimal displacement of the moderating medium, while simultaneously providing volumetric resolution of the average neutron thermalization along three-coordinate axes within the moderator–detector assembly (see Fig. 1). Three-dimensional resolve is important in improving the source identification accuracy (and in increasing the number of detector responses one can unfold against for absolute neutron energy determination), while also providing the ability to achieve directional resolution. The efficacy of all the analysis methods described here is based on the uniqueness (between various neutron source types) of the measured intensity as a function of three-dimensional position in the moderating medium (*vide infra*). Based on mean free path in common moderating media, the volumetric resolution for thermal and epithermal incident and scattered neutrons should be no larger than 1 cm^3, which forms the most restrictive design constraint. While state-of-the-art gaseous, doped-plastic, doped-glass, and doped-liquid thermal neutron detectors may be capable of meeting a small volume, their thermal neutron detection efficiency density is a factor of at least five times lower than advanced semiconductor-based detectors, especially when the readout electronics are also considered [8]. It is for these reasons, in addition to technological maturity, gamma-ray insensitivity, and availability, that the micro-structured neutron detectors (MSNDs) [3] have been chosen for use in this work.

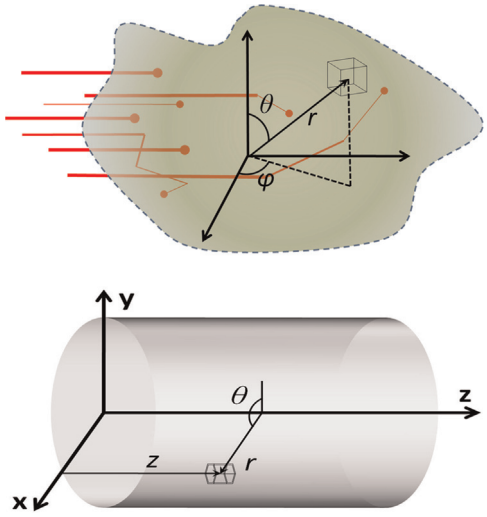

Fig. 1. Illustration of free neutrons thermalizing in a moderating medium, emphasizing the concept of volumetric resolution to better than 1 cm^3 along three coordinate axes (TOP). Illustration of a cylindrical moderator, and cylindrical coordinate system (BOTTOM).

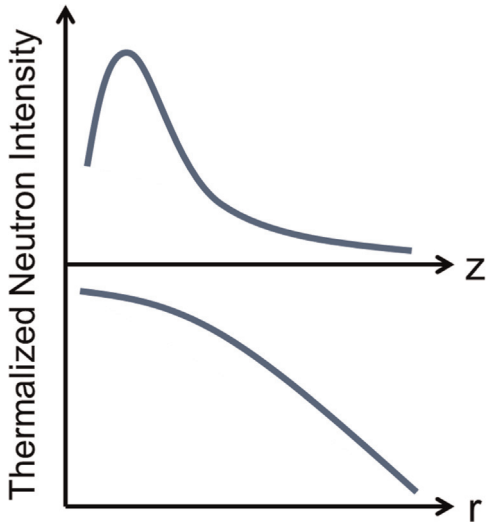

Fig. 2. A heuristic illustration of the thermalized neutron intensity distribution as a function of the axial and radial position in a cylindrical moderator in cylindrical coordinates. Neutrons with a Watt energy spectrum are assumed to be incident on the front face of a cylindrical moderator ($z=0$ is the front face) and uniformly distributed over r.

2.2. Theory of operation

Passively searching for and/or identifying neutron sources in non-proliferation applications requires the collection and analysis of one or more free neutron properties with high efficiency and energy sensitivity. To measure the neutron dose equivalent for health physics applications, identify one or more neutron sources, or determine the relative direction of a neutron source, analysis of the free neutron signature is one of the most powerful means. A high intrinsic and absolute neutron detection efficiency is important given the limited time available for measurement in these operational environments and energy sensitivity is crucial to neutron source identification and measuring the neutron dose equivalent [1,23]. Only the moderating-type neutron spectrometers are capable of enabling resolution of free neutron kinetic energy over the 10^{-8}–10^{1} MeV energy range while maintaining hand-held portability [1,7,23].

Although spectral deconvolution (unfolding) can be used to determine absolute neutron energy, relative or proportional signatures can provide as much or more information by template matching (measuring the degree of correlation of) the calibrated intensity profile to an absolute incident neutron energy signature (i.e., thermalized neutron intensity as a function of one or more axes in a moderating medium). Further, analysis of proportional signatures does not carry the computational overhead or assumptions required in solving the classically underdetermined and ill-conditioned inverse problem [10,11]. To measure quantities proportional to free neutron kinetic energy using the moderating mechanism, it is critical to design an instrument configuration whose sensitivity between incident spectral features and unique thermalization is maximized. To accomplish this connection, a combination of tuned scattering and absorption materials with thermal neutron detectors is required, and is discussed in detail below.

Fig. 2 shows starting point in understanding how the thermalized neutron intensity can be used as a signature of the incident neutron spectrum or the neutron source's location relative to the instrument. It is the spectral fingerprint (intensity as a function of one or more coordinate axes) uniqueness and intrinsic efficiency values, that serve as metrics for the process by which the instruments reported here are iteratively designed. Absolute neutron detection efficiency, which is determined by the area onto which the neutrons impinge, is not an essential feedback criteria of the

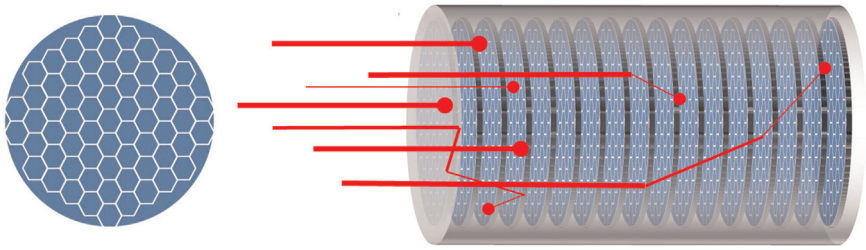

Fig. 3. LEFT – illustration of a MSND board with hexagonal patterning to form a 2-D detector array with approximate radial symmetry. RIGHT – an axial stack of 2-D detector arrays, separated and embedded by neutron moderator.

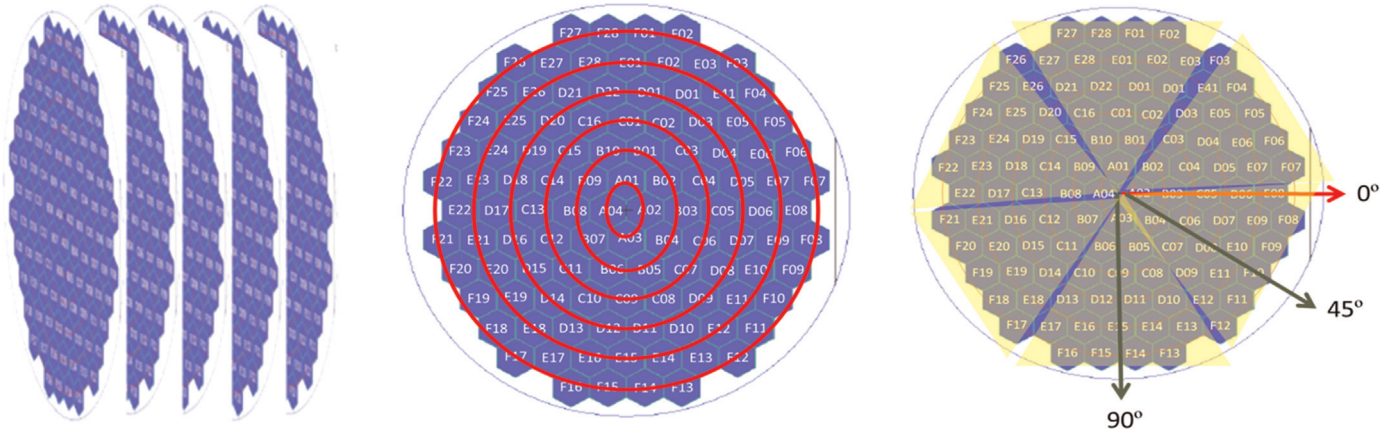

Fig. 4. Example illustrations of detector plane intensity summations vs. axial position (LEFT), vs. radius (MIDDLE), and vs. angular sector (RIGHT).

designs considered here; rather, energy-dependent intrinsic neutron detection efficiency, that normalizes area, is used. In this work, an instrument's intrinsic neutron detection efficiency to a particular neutron source spectrum, S, (e.g., bare ^{252}Cf, AmBe moderated by 1 in. of HDPE, etc.) is defined as:

$$\eta_{int}(S) = \frac{N_{det}(S)}{N_{inc}(S)} \quad (1)$$

where $N_{det}(S)$ is the total number of neutrons detected by the instrument from source S and $N_{inc}(S)$ is the total number of neutrons from source S that impinge upon the instrument volume. Fig. 2 shows that a Maxwellian-type neutron energy spectrum will cause a reproduction of that curve shape as a function of the axial position into the moderator, and that neutron scatter and escape will cause a drop-off in intensity as a function of radius. In this simplified example, the axial and radial distributions yield a signature of the neutron source that can be compared against reference intensity distributions. The problem is then how to design the detector–moderator assembly to best resolve these signatures and/or use the captured data to generate more complex distributions for comparison using source spectra of interest to the application.

2.3. Detector and moderator design

Based on the need to detect thermalized neutrons along three-coordinate axes in $\leq$1-cm^3 voxels in a moderating medium with axial symmetry (e.g., Fig. 1 BOTTOM), the instrument design initially converged on a 2-D array of pixelated detectors (Fig. 3 LEFT) that could be stacked axially to yield a 3-D array (Fig. 3 RIGHT). With each detector read out individually, thermalized neutron intensity can be summed for any coordinate, product of coordinates, or approximate volume (e.g., quadrants, octants) that best fits the application needs (see Fig. 4). For crude directional analysis, octant summing is useful (e.g., neutrons are incident from the forward-right-up position), and for crude source identification, summing each wafer plane and plotting the intensity vs. axial position can be useful (Fig. 2 TOP). To enable space-filling and approximate radial symmetry, a hexagonal pattern (Fig. 3 LEFT) was chosen for the first instrument design and build; later instruments used a square detector shape and square 2-D assembly to reduce the build complexity. In all, four instruments of varying mass and detector arrangement were designed, built, tested and will be discussed and compared.

In addition to the individual detector shape, the 2-D detector array design requires finding the optimal thermal neutron detection efficiency, active area, summed area, and summed shape(s). However, the overall instrument optimization process is ultimately determined based on the intimate relationship between detector and moderator, in reference to the source spectra of interest to the application and method of operation. Therefore, the design of the detectors should be made in the context of the overall instrument, in light of its concept-of-operations and the expected spectral distribution, including environmental scattering factors.

For simplicity, the source spectra used to optimize the instrument designs described here are that of bare ^{252}Cf [9] and bare AmBe [9]. Although the use of other sources, including moderated variants thereof, would follow the same procedure, bare ^{252}Cf and AmBe were chosen due to the similarities of their induced responses in moderating-type neutron spectrometers. Operationally, the instrument can be carried or set down for measurement. Neutrons can be incident from any direction when in source search mode, however, most of the source neutrons must enter the front cylinder face to optimally perform the identification analysis while in spectral mode. It is not absolutely required that the front face represent the reference datum point, since a signature can be developed for any incident angle relative to the long-axis of a cylindrical moderator–detector assembly; the downside for non-longitudinal incident neutrons is a lower net identification certainty, the discussion of which is outside the scope of this work. It is

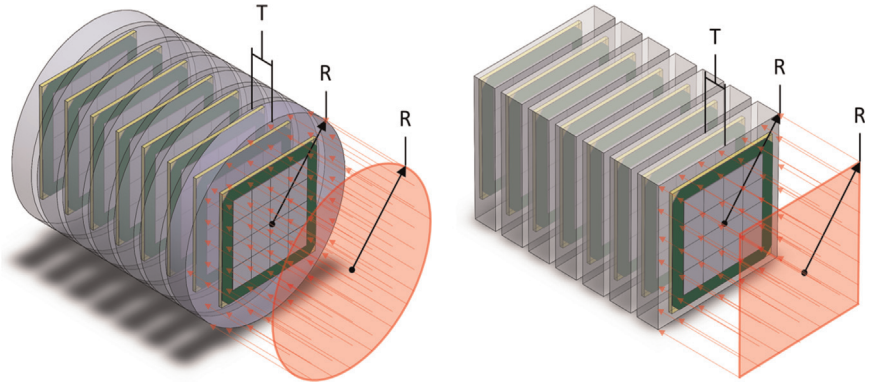

Fig. 5. Renderings of the cylindrical (LEFT) and rectangular prism (RIGHT) moderator geometries with eight 4×4 arrays of 4-cm^2 detectors, and the thickness and radius of the moderator slabs indicated. The red plane represents the neutron source used in the simulations to produce the results in Fig. 6. (For interpretation of the references to color in this figure legend, the reader is referred to the web version of this article.)

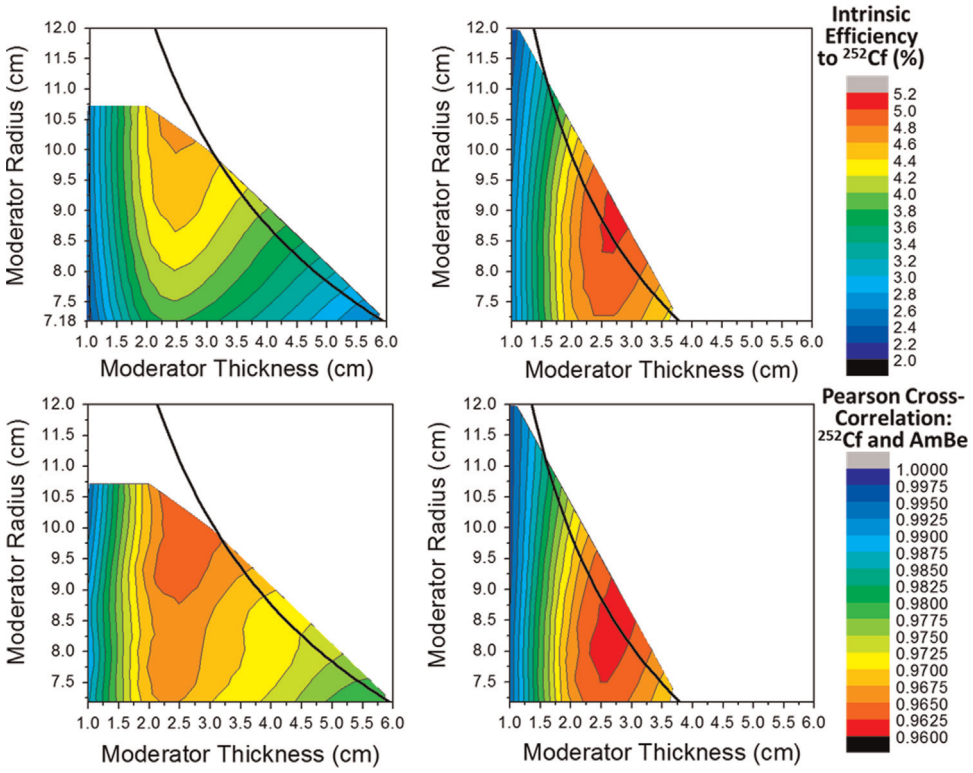

Fig. 6. Results of the simulated intrinsic neutron detection efficiency to bare ^{252}Cf for the rectangular prism (TOP LEFT) and cylindrical (TOP RIGHT) geometries, with a common color scale (red indicating maximum intrinsic efficiency). And results of the simulated spectral sensitivity metric (^{252}Cf–AmBe spectral difference) for the rectangular prism (BOTTOM LEFT) and cylindrical (BOTTOM RIGHT) geometries, with a common color scale (red indicating minimum Pearson correlation). The thick black line in each plot is an iso-mass curve, indicating the radius and thickness combinations that yield a total moderator+detector board weight of 10 lb. (For interpretation of the references to color in this figure legend, the reader is referred to the web version of this article.)

in this case, however, that a spherical geometry could be the best theoretical design due to 3-dimensional symmetry.

The design work discussed here is based on the simultaneous optimization of: (1) the intrinsic efficiency to bare ^{252}Cf (spontaneous fission being the neutron source type of interest to most applications), and (2) the ability to spectroscopically differentiate ^{252}Cf from AmBe (representing the ability to distinguish spontaneous fission sources from (α, n) neutron sources). Using (2) as a measure of the signature sensitivity, the efficacy of varying analysis techniques for each moderator–detector design type can be compared systematically. Source differentiation is an operational feedback tool analogous to energy resolution; when the spectral fingerprint between two sources or source configurations is most different, the energy resolution (in the most relevant energy range) or equivalent quantity should be optimal.

To perform the signature (or energy) sensitivity analysis for proposed instrument designs, a one-dimensional cross correlation analysis is used to provide an operational optimization metric. In this case, the Pearson product-moment cross-correlation coefficient [12] is used to yield a "score" between the axial intensity distributions created from a simulation of bare ^{252}Cf neutrons and a simulation of bare AmBe neutrons incident on the front face of the instrument. The Pearson correlation, r, (Eq. (2)) results in a value in the range $[-1, 1]$ which is a measure of linear correlation (similarity) between the two spectrometer responses, where $r=1$ indicates a total positive correlation (the signatures are exactly the same), $r=0$ indicates no correlation (the signatures are entirely different), and $r=-1$ indicates a total negative correlation (the signatures are exactly opposite). Therefore, the energy sensitivity of a proposed instrument design is optimal when this correlation

is minimized (i.e., when the two signatures are least similar and can be more easily differentiated).

$$r_{Cf,AmBe}(z) = \frac{1}{n} \bullet \sum_{i=1}^{n} \frac{N_{Cf}(z_i) - \overline{N_{Cf}(z)}}{\sigma_{N_{Cf}(z)}} \bullet \frac{N_{AmBe}(z_i) - \overline{N_{AmBe}(z)}}{\sigma_{N_{AmBe}(z)}} \quad (2)$$

where $N_{Cf}(z) = \begin{bmatrix} N_{Cf}(z_1) \\ \vdots \\ N_{Cf}(z_n) \end{bmatrix}$ is the ^{252}Cf response, $N_{AmBe}(z) = \begin{bmatrix} N_{AmBe}(z_1) \\ \vdots \\ N_{AmBe}(z_n) \end{bmatrix}$ is the AmBe response,

$\overline{N(z)}$ is the average of $N(z)$, and $\sigma_{N(z)}$ is the standard deviation of $N(z)$.

In order to optimize between the maximum intrinsic efficiency and minimum Pearson correlation metrics for the second and third instrument designs, numerous simulation series were conducted using the Monte Carlo *N*-Particle transport code (MCNP5). For each of the simulation series described here, although most other available parameters (e.g., moderator thickness, radius, and material) are varied within the design constraints (size, weight, cost, etc.), the MCNP representation of the detector boards remains unchanged and eight detector boards were used in each simulation (unless otherwise stated). Each of the eight detector boards consists of a 4×4 square array of 2-cm $\times$ 2-cm MSNDs. Each detector array is covered in front with an aluminum shield and mounted on a 10.16-cm $\times$ 10.16-cm FR-4 (E-Glass) printed circuit board (PCB) with all circuit components mounted to the side opposite the detector array (see Fig. 5).

The MSNDs are comprised of Si diodes, etched to form trenches and backfilled with ^{6}LiF powder; they yield an empirical thermal neutron detection efficiency of $\eta_{\text{th}} \approx 22\%$. The MSND detection mechanism has been described in detail previously [13]. To reduce computation time for the MCNP simulations described in this work, it was necessary to simplify the geometrical representation of the MSNDs. Each MSND was modeled as one 2-cm $\times$ 2-cm $\times$ 0.0525-cm rectangular prism (true MSND outer dimensions) containing both ^{6}LiF and Si, and the appropriate ratio of ^{6}LiF to Si was determined by matching the simulated and empirically measured thermal neutron detection efficiencies. To accomplish this, several preliminary simulations were run in which thermal neutrons (approximated by a Maxwellian distribution with a temperature parameter of 0.0257 eV), emitted uniformly from a planar source, were directed toward the MSND model. Since the neutron detection transduction mechanism of the MSNDs depends upon the reaction ${}^{6}_{3}Li^{3} + {}^{1}_{0}n \rightarrow {}^{4}_{2}\alpha + {}^{3}_{1}t$, the number of (n,t) reactions (i.e., neutron capture reactions in which tritons, ${}^{3}_{1}\text{Ha}^{1}$ nuclei, are produced) occurring in the lumped MSNDs were tallied (counted) in each simulation, and the thermal neutron detection efficiency, ηth, was calculated by

$$\eta_{\text{th}} = \frac{N_{(n,t)}}{N_{\text{th}}} \quad (3)$$

where $N_{(n,t)}$ is the total number of (n,t) reactions occurring in the lumped MSNDs and *N*th is the total number of thermal neutrons that impinge upon the Lumped MSNDs. Keeping the percentages of ^{6}Li and F equal, the ratio of ^{6}LiF to Si was adjusted in each simulation until 22% thermal neutron detection efficiency was achieved.

2.3.1. Moderator geometry and dimension optimization

Although one could consider many other geometries, only the cylindrical and rectangular prism moderator geometries were designed and built (Fig. 5) using high-density polyethylene (HDPE). A spherical design offers the most flexibility and can intrinsically mitigate the effect of environment-scattered or multi-directional neutrons, and conical designs may show merit, but their manufacturing complexity and/or required thermalization mass is too high. Fig. 6 shows the simulated intrinsic neutron detection efficiency and spectral sensitivity for both the cylindrical and rectangular prism designs as a function of moderator radius, *R*, and thickness, *T*, between each of the eight detector boards. In the case of the rectangular prism, the radius is defined, as shown in Fig. 5, by the distance from the center to the corner of the moderator front face.

The instrument optimization and analysis methods used to create Fig. 6 serve as a primary theoretical baseline and operational feedback tool for the instrument designs described in this work. As stated previously, the 4×4 array detector boards are considered here to be a fixed design parameter for investigating the effects of moderator geometries and dimensions on the aforementioned operational performance metrics for detection efficiency and source identification (energy sensitivity). The limit of eight detector boards per instrument is estimated based on conservatively-projected cost limitations, forming another fixed design parameter. Holding these two parameters constant, the physical moderator dimensions shown in Fig. 5 are varied under an active weight constraint of 10 lbs, and simulated for a course grid of discrete radius and thickness combinations (representing single (x, y) points in each plot in Fig. 6). Intrinsic neutron detection efficiencies to bare ^{252}Cf and Pearson correlations between bare ^{252}Cf and bare AmBe instrument responses are then calculated for each discrete radius and thickness combination and plotted in a third (metric) dimension. A three-dimensional interpolation is then applied to the data, indicating regions of the tunable parameter space that may warrant further exploration. These promising regions are then broken down into finer grids of discrete points for subsequent simulation, and the

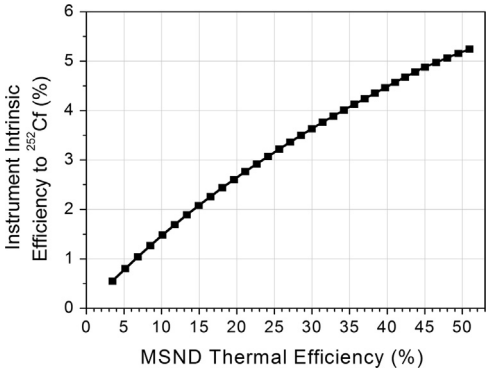

Fig. 7. Simulated instrument intrinsic detection efficiency to ^{252}Cf as a function of MSND thermal neutron detection efficiency.

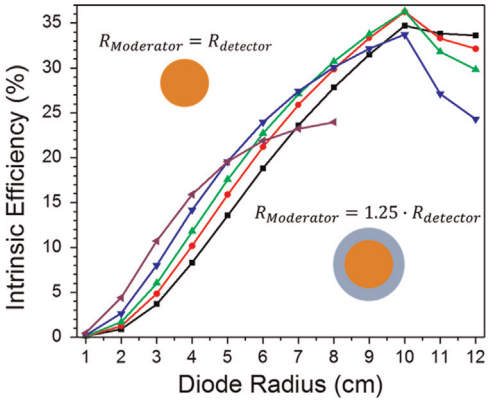

Fig. 8. Intrinsic neutron detection efficiency to ^{252}Cf as a function of the detector (diode) radius for varying detector to moderator radii ratios (■ $R_{moderator} = R_{detector}$, ● $R_{moderator} = 1.125 \cdot R_{detector}$, ▲ $R_{moderator} = 1.25 \cdot R_{detector}$, ▼ $R_{moderator} = 1.5 \cdot R_{detector}$, ◀ $R_{moderator} = 2 \cdot R_{detector}$).

process is repeated until no practically significant improvement can be made toward the desired optimization metric. This optimization technique is explored further and utilized to a fuller extent in following sections.

In analysis of Fig. 6, the most immediately apparent result is that, for an active instrument weight of less than 10 lb, the cylindrical moderator geometry outperforms the rectangular prism geometry for both operational metrics. Since portability is of primary concern to both nuclear nonproliferation and health physics applications, the cylindrical geometry is clearly more optimal for meeting the application needs under the simplifying assumptions made here. It is also significant (and serendipitous) to note that, for both geometry types, the optimal moderator thickness is roughly the same for both performance metrics, indicating that simultaneous optimization may be possible without significant tradeoffs to either metric.

2.3.2. Detector efficiency optimization

Commercially available microstructured semiconductor neutron detectors are capable of thermal neutron detection efficiencies in excess of 44% [14,21]. To explore the effect of increasing thermal neutron detector efficiency of the constituent MSNDs on the intrinsic neutron detection efficiency of a cylindrical spectrometer design, a series of simulations was conducted in which neutrons from a bare ^{252}Cf source were incident upon the front circular face of a moderator–detector assembly with thirty 5-inch diameter cylindrical detector boards, separated axially by 1-cm of HDPE with 5-in. diameter (initial **5C** design, Fig. 3, discussed further in Section 3). The thermal neutron detection efficiencies of the constituent MSNDs were varied in each simulation from 3% to 51%. Fig. 7 shows that as the thermal detection efficiencies of the MSNDs increases above 22% there is a diminishing return to the instrument intrinsic efficiency to bare ^{252}Cf. Quantitatively, the intrinsic neutron detection efficiency more than quadruples (from 0.669% to 2.85%) when using a 22% detector over a 4% detector, while only increasing by a factor of 1.68 (from 2.85% to 4.79%) when using a 44% detector over a 22% detector. Due to this diminishing return in intrinsic efficiency, the instruments designed in this work were held to 22% thermal neutron detection efficiency MSNDs.

2.3.3. Moderator radius to detector radius ratio optimization

As shown in Fig. 2 (BOTTOM), in the case that the detector plane is the same radius or area as the axially symmetric moderator, the intensity of neutron counts (from normal incident on the front cylinder face) fall off as a function of radius. If a neutron reflecting material is placed outside of the outer detector radius, some neutrons can be re-scattered or reflected inward and the intrinsic neutron detection efficiency can increase. Fig. 8 shows how an instrument's intrinsic efficiency to bare ^{252}Cf changes as a function of outer detector radius for various moderator-to-detector radius ratios. In these simulations, high density polyethylene is used as both the central moderator and reflector. In all simulations with an outer detector radius less than 5 cm, the intrinsic efficiency increases as the moderator-to-detector radius ratio increases. Above a 5-cm outer detector radius the intrinsic efficiency increase slows and reaches a maximum of 36% at a 10-cm outer detector radius for the 1.125 and 1.25 moderator-to-detector radius ratios. The falloff above a 10-cm outer detector radius for all moderator-to-detector ratios is due to the moderator radius being larger than the average mean free path of the bare ^{252}Cf neutrons in high density polyethylene. This leads to increased neutron absorption by hydrogen nuclei in the moderator volume ($^1_0n^0 + {}^1_1H^1 \rightarrow {}^1_2H^2 + \gamma$ (2.1MeV)). For a portable instrument with cylindrical symmetry and total weight of ~15-lb, the moderator volume, at maximum, would be restricted to a 7.6-cm radius and 30-cm length. To achieve the highest intrinsic efficiency (not necessarily the highest absolute efficiency) for the cylindrical geometry (~15%) and total weight of ~15-lb, the detector radius would not exceed 3.8-cm.

Table 1
Potential instrument moderator material salient properties.

Moderator	Chemical formula	H-Conc. (Atoms/cm^3)	C-Conc. (Atoms/cm^3)
High-density polyethylene	$(C_2H_4)_n$	8.07702E+22	4.29172E+22
Polystyrene	$(C_8H_8)_n$	4.85521E+22	4.85521E+22
Polysulfone	$(OC_6H_4OC_6H_4SO_2C_6H_4)_n$	2.76176E+22	4.14264E+22

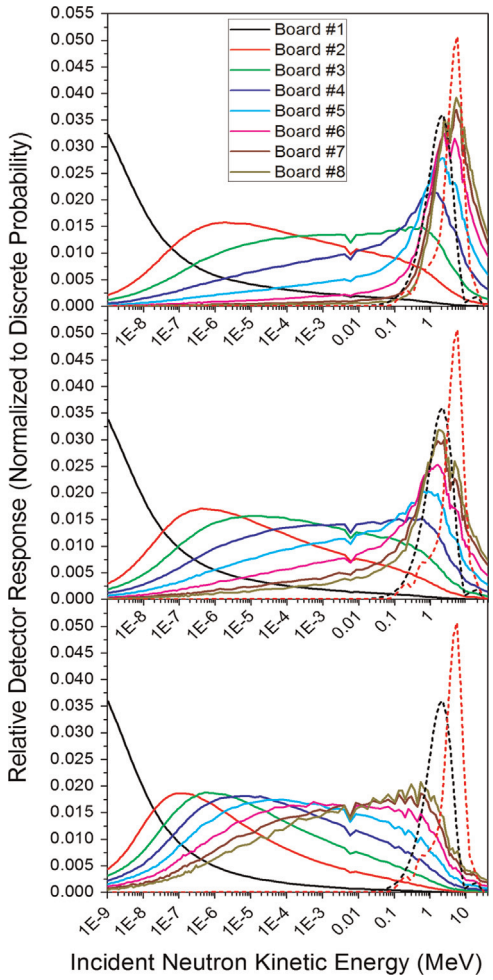

Fig. 9. Shown (ALL) are normalized detector-board-summed response functions (solid lines) of instruments with a cylindrical moderator design with 7.62-cm radius and 3.6-cm thickness, as shown in Fig. 5, with 8 rectangular detector boards. Simulated moderator materials were varied with HDPE (TOP), polystyrene (MIDDLE), and polysulfone (BOTTOM). In each case, the first detector board (most sensitive to the lowest energy neutrons) is represented in black and is leftmost, while the last detector board (most sensitive to the highest energy neutrons) is represented by olive and is rightmost. Normalized ^{252}Cf (– – –) and AmBe (– – –) neutron emission spectra are also included in each plot for reference.

2.3.4. Moderator type optimization

A major goal of this work is to design an instrument that will yield the most unique distribution of detected thermalized neutrons while also maintaining the highest possible intrinsic efficiency. Since the type of neutron moderating material used can greatly influence both of these operational characteristics, it is important to consider the role of moderators other than high density polyethylene (HDPE). HDPE is a popular neutron

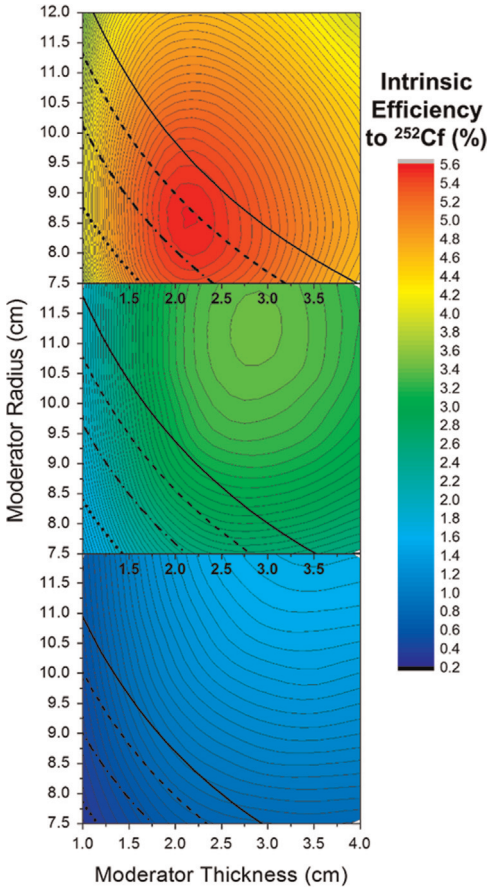

Fig. 10. Instrument intrinsic efficiency to ^{252}Cf as a function of moderator radius and thickness using HDPE (TOP), polystyrene (MIDDLE), and polysulfone (BOTTOM), with iso-mass curves indicating the radius and thickness combinations that yield a total moderator+detector board weight of 6-lb (···), 8-lb (−•−•), 10-lb (− − −), and 12-lb (−).

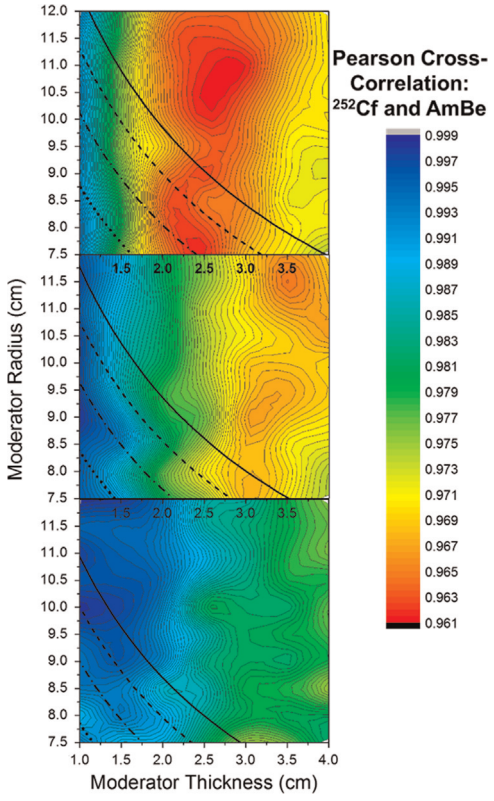

Fig. 11. Pearson cross-correlation between ^{252}Cf and AmBe instrument responses as a function of moderator radius and thickness using HDPE (TOP), polystyrene (MIDDLE), and polysulfone (BOTTOM), with iso-mass curves indicating the radius and thickness combinations that yield a total moderator+detector board weight of 6-lb (···), 8-lb (−•−•), 10-lb (− − −), and 12-lb (−).

moderating material because it is inexpensive, readily available, mechanically strong but easily machinable, and resilient to most environmental factors. Its hydrogen concentration by volume is very high (i.e., 8.07702E+22 Atoms H/cm^3), which is important for neutron scattering and moderation. However, could a very high hydrogen concentration also be detrimental to thermal and lower-epithermal energy resolution, as neutrons in these energy ranges can be thermalized and detected with little traverse into the instrument detector layers? Or conversely, could a higher hydrogen concentration material, or possibly high carbon containing, help to improve the thermalized intensity distribution (i.e., signature of higher-epithermal or fast neutrons) by better physical separation of the higher energy neutrons detected?

To help answer these questions, simulations were performed using high-density polyethylene (HDPE), polystyrene, and polysulfone moderator materials, all in the same instrument configurations, in order to study the effect of varying hydrogen and carbon concentration on the overall performance of the instrument; a summary of each moderator's salient properties is shown in Table 1. Fig. 9 shows how the detector response functions vary for HDPE, polystyrene, and polysulfone in one of the tested instrument configurations (7.62-cm radius and 3.6-cm thickness, as defined in Fig. 5 LEFT). Figs. 10 and 11 show constructed using the optimization procedures described in Section 2.3.1; however, the weight restriction of the initial data point grid was relaxed and the radius-thickness parameter space was explored more thoroughly. Fig. 10 shows the effect that the varied moderator type had on the instrument's intrinsic detection efficiency to bare ^{252}Cf. Fig. 11 shows how the spectral sensitivity metric (Pearson cross-correlation between bare ^{252}Cf and bare AmBe instrument responses, Eq. 2) is affected by the different moderators.

The response functions' peak positions and full width at half maximums (FWHM) provide another means by which spectral sensitivity can be analyzed [15]. As an example, if all of the response functions were non-overlapping delta functions, the energy resolution would be perfect at each response's energy but the sensitivity would be limited only to those energies and, hence, the efficiency would be very small and unacceptable. On the other side, if all of the response functions span the entire energy range, and have the same shape and relative efficiency, the system yields no energy resolution, which is also unacceptable. The desired response functions are those that are narrow in energy, numerous, next to each other with little overlap, and cover the energy range of interest to the application.

As shown in Fig. 9, as the atomic ratio of hydrogen to carbon is decreased from H/C=2.0 (HDPE) to H/C=1.0 (polycarbonate) to H/C=0.6 (polysulfone), the peak position of each detector board response function (with the exception of the front board which has no anterior moderator) is shifted to a lower energy. While this shift to lower energies provides more even coverage of the entire 10^{-9}–40 MeV energy range shown in Fig. 9, the vast majority of neutron emissions from bare ^{252}Cf and AmBe (dashed black and red lines in Fig. 9 respectively) exceed 10^{-1} MeV. The effects of the low energy shift on spectrometer performance are evident from Figs. 10 and 11, which depict a significant decrease in instrument intrinsic efficiency to bare ^{252}Cf and increase in Pearson correlation between bare ^{252}Cf and AmBe instrument responses with decreasing hydrogen-to-carbon atomic ratio. However, while these trends are detrimental to instrument performance in application to bare spontaneous fission and (α, n) neutron sources, they may

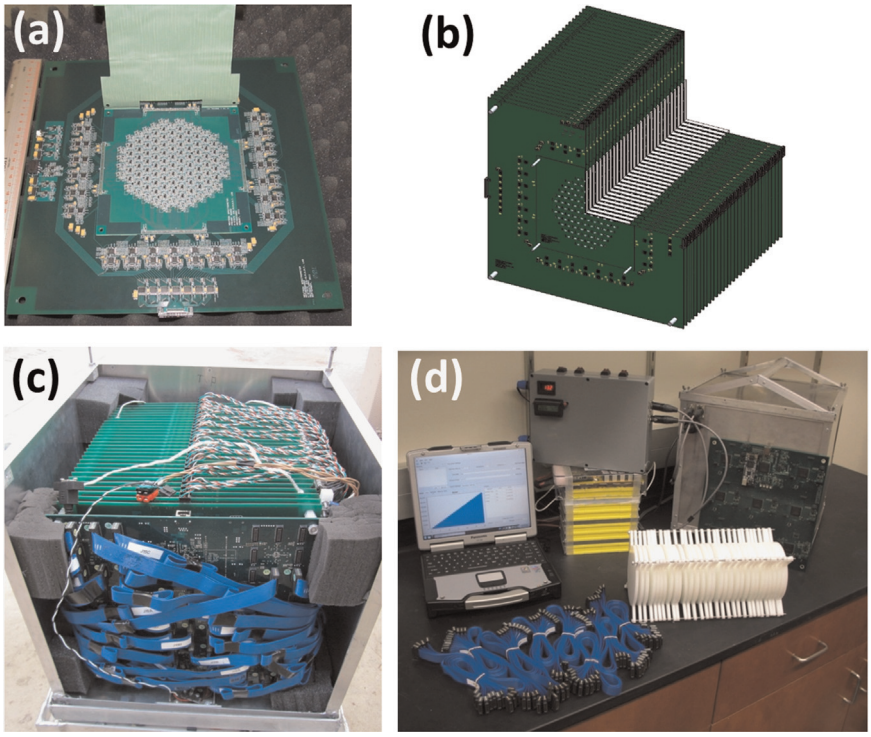

Fig. 12. Photographs and renderings of the **5C** system showing (a) an individual printed circuit board with mounted microstructured neutron detector die, (b) assembly cut-away view showing 30 alternating board–moderator pairs, (c) assembled instrument with the top and back cover removed, and (d) instrument case, HDPE moderator, cables, battery, power supply, battery, and digital signal processing board.

be beneficial to performance in application to moderated variants thereof. After evaluating the effect of this low energy shift on moderated source types, it was determined that the performance benefits for moderated neutron sources are far outweighed by the detriment to bare neutron source performance, and HDPE proved to be the most optimal for a wider range of relevant applications.

2.3.5. The role of absorbers

Just as varying the moderator type can change the macroscopic neutron scattering distribution, and hence alter the response, intrinsic efficiency, and spectral sensitivity, so too can neutron absorbing materials. As shown in prior work for the long counter and similar geometries to those considered here [16–23], the addition of absorbers can provide two important physical attributes. First, if the neutron absorbers are tuned to capture neutrons at an energy threshold and/or resonance, and those thresholds cover many decades of energy and are strategically placed in space (e.g., stacked), they can act to filter neutrons by energy; this trait alone (i.e., without moderator) creates a crude neutron spectrometer, and can enhance a moderating-type neutron spectrometer. Second, neutron absorbers placed behind stacked detectors, in a moderating-type neutron spectrometer, act to capture some backscattered neutrons. Most backscattered neutrons cause a loss of energy resolution as they defeat the axial depth dependence of forward down-scattering. However, absorbers simultaneously decrease the intrinsic neutron detection efficiency of the instrument and usually cause secondary reaction products (e.g., capture gamma-rays) so their use should be carefully considered in light of the gamma-ray blindness or discrimination capability of the neutron detectors. In the case of the instruments described here, neutron absorbers were serendipitous and unavoidable, as the semiconductor-based neutron detectors were mounted to 0.81-mm (0.032 in.) thick FR4 printed circuit board (PCB), containing ^{79}Br, ^{81}Br, and ^{10}B. The FR4 PCBs absorb 16% of the thermalized neutrons at each detector layer, improving energy resolution at the cost of decreased intrinsic neutron detection efficiency.

3. Instrument results

Based on the design methods described above, the four moderating-type neutron spectrometers were built to test and compare the empirical response of different instrument configurations. Here forward, the instrument systems will be referred to as the 5-in. cylinder (**5C**), shown in Fig. 12, the 6-in. cylinder (**6C**), shown in Fig. 13, the 4-in. rectangular prism (**4RP**), shown in Fig. 15 and the 4-in. cylinder (**4C**), shown in Fig. 16.

The **5C** was the first instrument built; comprised of thirty detector boards, each containing 108 hexagonally-shaped 1-cm^2 MSNDs and arranged into the pattern shown in Fig. 4. On each detector board, all 108 MSNDs were etched as a single monolith into a 5-in. diameter silicon wafer and read out individually through coaxial cables to a digital signal processing board, containing 8 field-programmable gate arrays for the 3240 total channels. When completed, the moderator and detector board assembly weighed 48-lb without the case, battery, power supply or laptop. Due to this nearly non-portable mass, overall complexity, and excessive number of channels (*vide infra*), the next three designs focused on reducing the overall mass and volume, while improving operational reliability and effectiveness.

In the **6C** and **4RP** designs, cable connections were removed and the power conditioning, battery, and computer were moved internal to the case. The detector daughter boards are composed of a 4×4 array of 4-cm^2 detectors, shown in Fig. 13a, with a connector that plugs directly into a motherboard above the moderator volume (Fig. 13c). Both the **6C** and the **4RP** designs contain eight daughter boards for a total of 128 individual detector channels per instrument, each channel being read into a single Xilinx Spartan

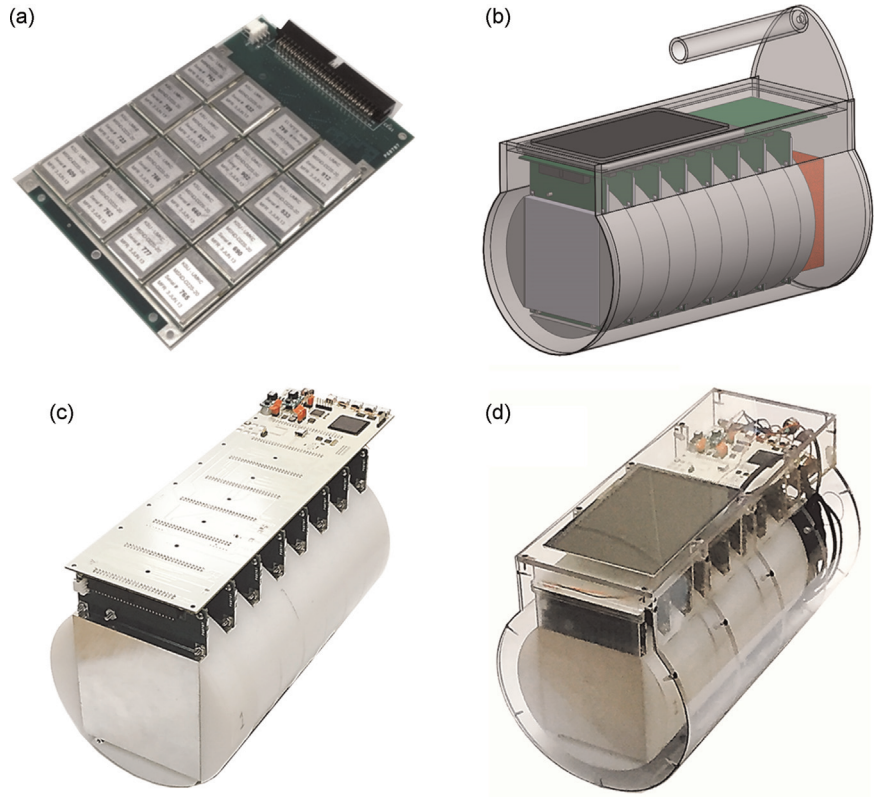

Fig. 13. Photographs and renderings of the **6C** system showing (a) an individual printed circuit board with mounted microstructured neutron detectors, (b) assembly view showing the eight boards with recessed moderator slabs, motherboard, Nexus 7 tablet, battery pack, and case (transparent), (c) assembled instrument with the case, Nexus 7 tablet, and battery packs removed, and (d) fully assembled **6C** neutron spectrometer.

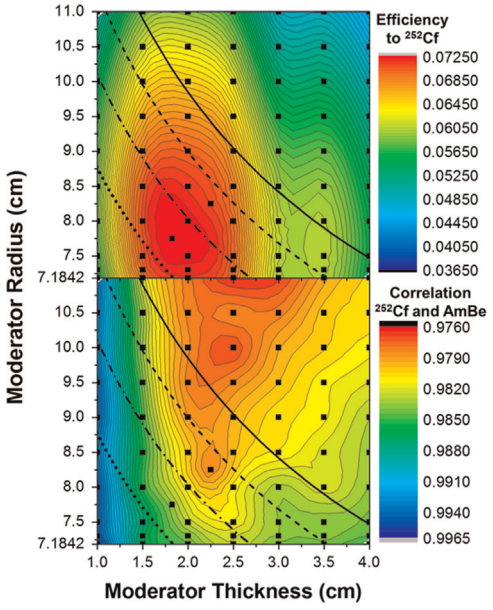

Fig. 14. 6C spectrometer intrinsic efficiency to ^{252}Cf (TOP) and Pearson cross-correlation between ^{252}Cf and AmBe **6C** spectrometer responses (BOTTOM) as a function of HDPE moderator radius and thickness, with iso-mass curves indicating the radius and thickness combinations that yield a total moderator+detector board weight of 6-lb (···), 8-lb (–•–), 10-lb (– – –), and 12-lb (–). • represent initially simulated data points, as well as optimal data points for each metric (< 10-lb).

3AN FPGA. A Nexus 7 tablet serves as the user display, information processor, and control center of the motherboard.

Using the optimization procedures described in Section 2.3.1, and restricting the total weight of the moderator and detector boards to be less than 10 lb as a design constraint, the optimal thickness and radius of the **6C** moderator slabs (as defined in Fig. 5 LEFT) was found to be 2.29 cm and 7.62 cm respectively, as shown in Fig. 14. This radius and thickness combination is a compromise between the optimal intrinsic detection efficiency, at $T=1.825$ cm and $R=7.75$ cm, the optimal spectral difference, at $T=2.25$ cm and $R=8.25$ cm, and practical availability, with more emphasis given to the intrinsic detection efficiency metric. It should be noted that the **6C** moderator slabs envelope the detectors, not just separate them (as portrayed in Fig. 5), which leads to a significant decrease in neutron leakage, despite the small increase in mass. Therefore, with the detector board recess accounted for, the total moderator slab thickness used was 3.6 cm (1.31-cm deep detector board recess, 2.29 cm between detector boards, as shown in Fig. 13b and c).

For the **4RP** spectrometer, the goal was to utilize the same motherboard as the **6C** but reduce the HDPE mass (from that of the **6C**) by keeping only the portion separating the detector layers, resulting in a rectangular prism geometry. In doing so, the total instrument weight dropped from 18.5 lb, for the **6C**, to 13.8 lb for the **4RP**; the moderator portion of the **4RP** weight was 3.4 lb. Using the same moderator radius/thickness optimization procedure, but with the definition given in Section 2.3.1 (Fig. 5 RIGHT) for the rectangular-prism radius, the optimal thickness of the HDPE for the **4RP** instrument was found to be approximately 2.75–3.0 cm. Therefore, the same moderator thickness as the **6C** design, 2.29 cm, could be used for the **4RP** design without significant detriment to either operational performance metric. Since reducing mass while retaining high intrinsic efficiency and spectral sensitivity is critical to the commercial adoption of this type of instrument, it is necessary to understand the tradeoffs between the **6C** and **4RP** moderator configurations (Fig. 15).

To consider even more dramatic tradeoffs in cost, mass, and complexity, the **4 C** moderating-type instrument was designed with a total weight restriction of < 9 lb and the use of only one 4-

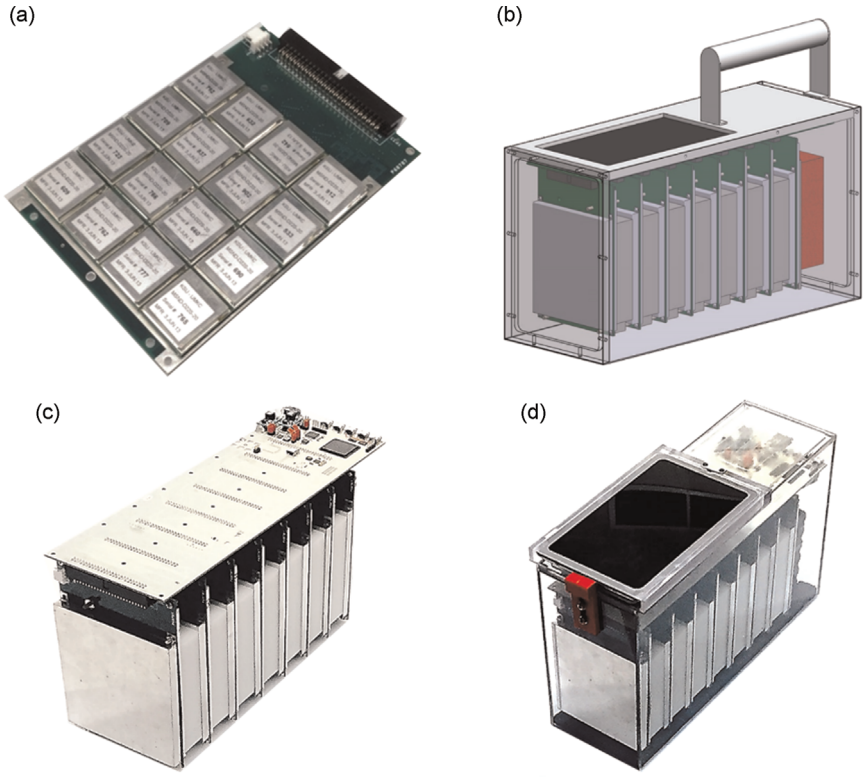

Fig. 15. Photographs and renderings of the **4RP** system showing (a) an individual printed circuit board with mounted microstructured neutron detector die, (b) assembly view showing the eight alternating detector–moderator pairs, motherboard, Nexus 7 tablet, battery pack, and case (transparent), (c) assembled instrument with the case, Nexus 7 tablet, and battery packs removed, and (d) fully assembled **4RP** neutron spectrometer.

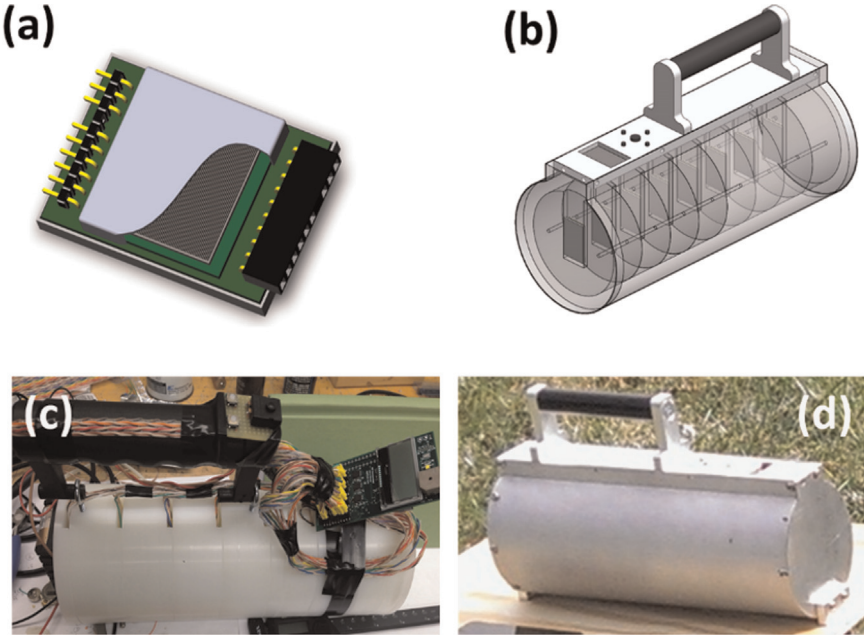

Fig. 16. Photographs and renderings of the **4C** system showing (a) an individual printed circuit board with single mounted microstructured neutron detector die, (b) assembly view showing the 8-MSNDs with recessed moderator slabs, motherboard, display, and case (transparent), (c) assembled instrument with the case, and battery packs removed, and (d) fully assembled **4C** neutron spectrometer.

cm^2 MSND (Fig. 16a) at each of the eight depths into the moderator volume (Fig. 16b). The same optimization process shown in Fig. 14 was used to find the optimal radius and thickness combinations for the intrinsic efficiency and spectral sensitivity. The optimization process yielded a 5-cm radius and 2.25-cm thickness for optimal intrinsic detection efficiency, and a 5-cm radius and 3-cm thickness for optimal spectral sensitivity. A radius of 5.08 cm and thickness of 2.29 cm were used for the actual fabrication of the moderator slabs, based on practical considerations such as the availability of materials, and the total moderator weight was 5.0 lb. Note that the optimal moderator dimensions for all design models were very similar, due to the predictable probabilistic nature of

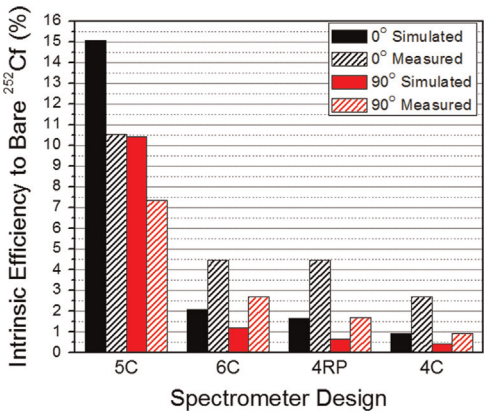

Fig. 17. Simulated and measured intrinsic efficiency to bare ^{252}Cf (in %) for each spectrometer model, from 0° (front face) incidence and 90° (side) incidence.

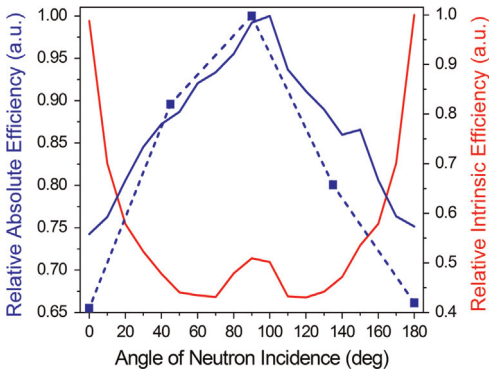

Fig. 18. 5C spectrometer simulated relative intrinsic efficiency (–), simulated relative absolute efficiency (–), and experimental relative absolute efficiency (– – –) to bare ^{252}Cf, as a function of neutron incident angle (in degrees). All efficiencies are normalized to allow for direct comparison.

neutron energy loss and scattering angle via elastic scattering interactions in the common moderator material under consideration (HDPE). While moderator shape and detector board type played minor roles, the small differences in optimal configurations was largely due to the progressively restrictive weight constraints imposed from the **6C** to the **4RP** and **4C** spectrometer designs.

3.1. *Intrinsic efficiency*[1]

The intrinsic neutron detection efficiency, for a particular energy spectrum, was defined in this work as the ratio of the number of neutrons detected to the number of source neutrons incident on the instrument moderator volume (Eq. (1)), represented as a percentage. This definition helps to normalize the results compared between instruments, as it partially accounts for the moderator dimensions. If the intrinsic neutron detection efficiency is reported for two or more faces of each instrument (e.g., front incidence and side incidence), a one-to-one comparison can be made between the detection systems. Further, one can use the intrinsic neutron detection efficiency to compute the absolute neutron detection efficiency for the source size and distance of interest to their application. This allows for direct comparisons between instruments with respect to the ability to passively detect neutron sources alone. To help put the values reported here in context, with an intrinsic efficiency to bare ^{252}Cf of ~4.5% for neutrons incident on the front face of the **6C** instrument (i.e., 182-cm^2 area), a 95% detection certainty of a 1E5-n/s source at 10-m distance could be made in 50 s.

The simulated and measured intrinsic neutron detection efficiency values to bare ^{252}Cf for each instrument are compared in Fig. 17 for front and side incidence (0° and 90° respectively). While the empirically measured intrinsic neutron detection efficiency values to bare ^{252}Cf for the **6C**, **4RP**, and **4C** spectrometers are, on average, 1.7% greater (1.4% relative) than their simulated values from both the front and side, the measured value of **5C** is 4.5% less (30.1% relative) than its simulated value from the front and 3.1% less (29.5% relative) than its simulated value from the side. In the case of the **5C** design, the MCNP simulations had to be significantly simplified due to the complexity of the detector electronics boards and did not account for the neutron capture properties of the FR-4 printed circuit board, resulting in a greater efficiency in simulation than experiment. In the case of the **6C**, **4RP**, and **4C**, the detector boards were simpler to model, allowing for the inclusion of the FR-4 PCBs and electronics in simulation, leading to the correct trends for these instruments, as shown in Fig. 17. The relatively small differences in magnitude between the simulated and measured efficiencies in these cases are mostly due to environmental scattering effects which were not included in simulation. Environmental neutron scattering leads to an increase in the number of thermalized neutrons impinging on the spectrometer volume and, in turn, a greater intrinsic neutron detection efficiency. The **5C** spectrometer achieves the highest overall efficiency values due to having a much larger total active detector area than the other instruments. For a more relative comparison, however, the instruments' intrinsic efficiency per cm^2 of total detector area can instead be considered. Viewing the experimental results at 0° (front face) incidence in this detector-area-normalized manner, the efficiency per unit detector area trends in the opposite direction; 0.00277% per cm^2 for the **5C**, 0.00876% per cm^2 for the **6C**, 0.00874% per cm^2 for the **4RP**, and 0.0841% per cm^2 for the **4C**. This demonstrates that although intrinsic detection efficiency was sacrificed to some degree with each design simplification (**5C**→**6C**→**4RP**→**4C**, in order of decreasing complexity) due to decreased moderator volume and/or detector area, the design optimization processes (discussed in previous sections) for each instrument were successful in mitigating these sacrifices by maximizing efficiency under each increasingly restrictive set of design constraints.

The simulated and measured angular dependence of the absolute neutron detection efficiency, and the simulated angular dependence of the intrinsic neutron detection efficiency, of the **5C** design are shown in Fig. 18, for bare a ^{252}Cf neutron source. In all cases, 0° indicates normal incidence on the front face of the instrument. The reason the intrinsic neutron detection efficiency is highest at 0° and 180° is that, for each of the instruments, much of the latter half of the 30-cm axial depth is used to thermalize incident neutrons from the ^{252}Cf source whose energy is in excess of 5 MeV. In the case of **5C**, the 12.7-cm moderator diameter is not sufficient to thermalize the majority of side-incident neutrons (90°). Absolute detection efficiency is highest for side incidence as the total cross-sectional area is more than a factor of 3 greater than the front face of the instrument. The low points in the intrinsic efficiency at ~55° and ~125° are due to the excess path length of FR4, and are only specific to the **5C** design.

3.2. *Identification*

To identify sources of neutron radiation, the instrument software utilizes the previously discussed Pearson product-moment

[1] All empirical intrinsic efficiency measurements reported here were collected with a bare ^{252}Cf source 100 cm from the instrument. Data was collected until the counting statistics for the overall instrument yielded less than 2% error. The instruments were positioned 120 cm above a concrete floor, 200 cm below a concrete ceiling, and 5 m from a single concrete wall facing the instrument to help minimize the asymmetry and overall detection of environmentally scattered neutrons. Finally, tests using a shadow shield validated that less than 5% of the detected neutrons were from environment scatter.

cross-correlation coefficient (Eq. 2). First, an extensive library of spectrometer responses (summed detector board counts as a function of axial depth $N(z)$) must be generated through either MCNP simulation or empirical measurement, and should include as many neutron source types and moderator/absorber configurations as is necessary for a given application. With this library of responses generated and uploaded to the spectrometer's software, live response data collected from an unknown source is then compared to each library response using the Pearson cross-correlation coefficient, r, and ranked to yield the closest matching source (i.e., the source type with the most correlated library response is chosen as the most likely source identity). This process is repeated and displayed to the user in one-second updates as the collected data accumulates.

To test the neutron source identification capabilities of the **6C** and **4RP** spectrometers under various moderator/absorber configurations as a function of both time and distance from the source, a series of experiments were planned and conducted in a large grass field (Fig. 19, TOP) at the Naval Surface Warfare Center Carderock Division in West Bethesda, Maryland. The neutron source used for the experiments was a 4.432×10^5-n/s ^{252}Cf source inside a thin moderating NIST-RG-LL-09-252-D sphere (Fig. 19A).

Lines were marked in the grass to indicate radial distances from the neutron source in 0.5-m increments, from 0.5–5.0 m, as shown in Fig. 19 (TOP). Measurements were then taken with both instruments at each distance, with the data collection time adjusted to ensure less than 5% count error. This set of experiments was then repeated 3 more times with additional moderator/absorber configurations: 1 in. of high density polyethylene surrounding the NIST sphere (Fig. 19B), four 50-lb sacks of H_3BO_3 (boric acid) tied around the NIST sphere (Fig. 19C), and 1 in. of HDPE plus four 50-lb sacks of H_3BO_3 tied around the NIST sphere (Fig. 19D). A summary plot of the results of these experiments is shown in Fig. 20 below. Neutron source libraries included

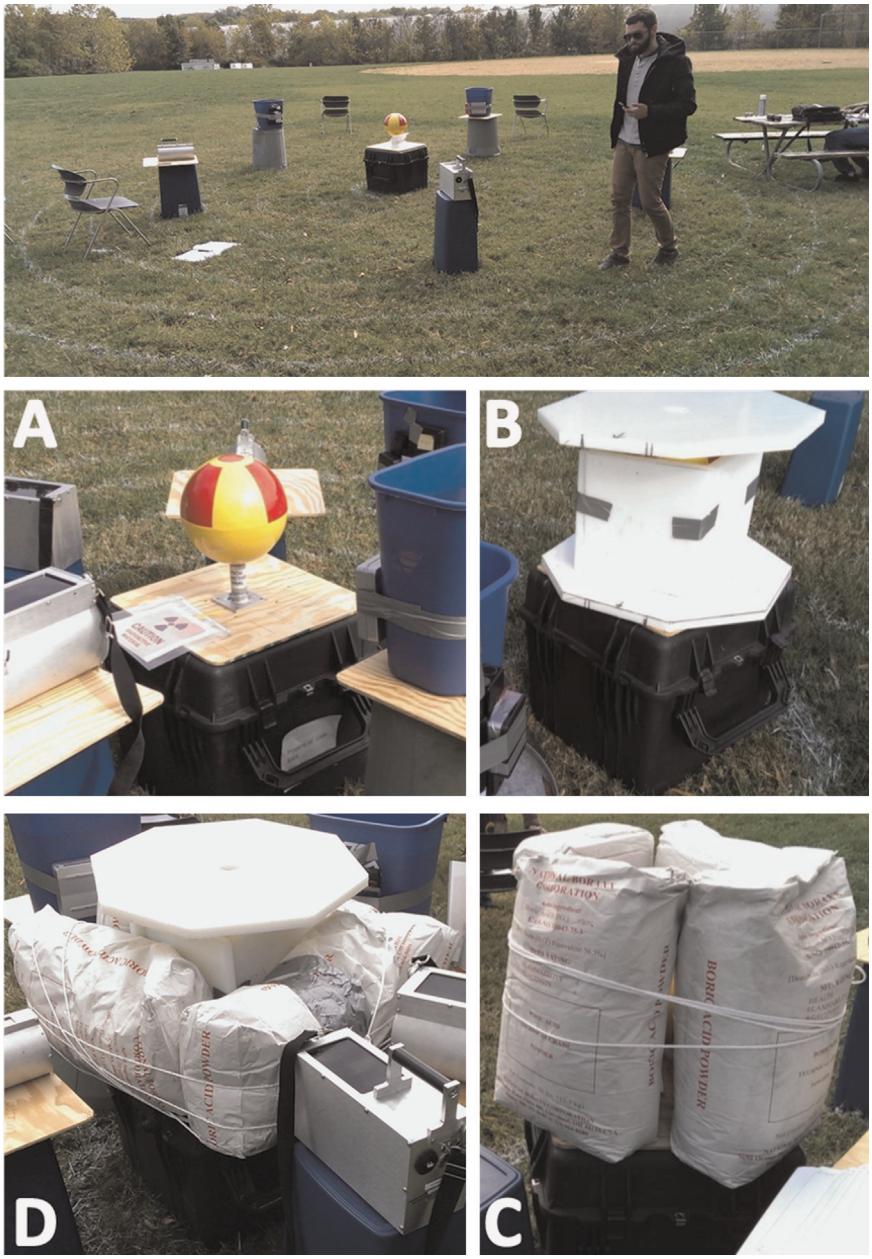

Fig. 19. Neutron source identification experimental setup (TOP) with lines indicating radial distances from the neutron source in 0.5-m increments. Neutron source+moderator/absorber configurations tested: (A) 4.432×10^5 n/s ^{252}Cf source inside moderating NIST-RG-LL-09-252-D sphere, (B) 1 in. HDPE surrounding (A), (C) Four 50-lb sacks of H_3BO_3 tied around (A), and (D) Four 50-lb sacks of H_3BO_3 tied around (B).

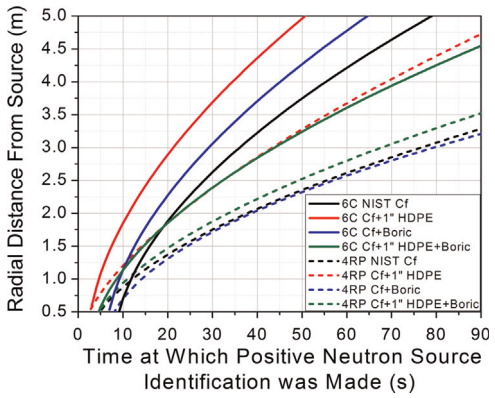

Fig. 20. Identification experiment summary plot. The time at which a positive neutron source+moderator/absorber identification was made (in seconds) is plotted as a function of radial distance from the neutron source (in meters). (For interpretation of the references to color in this figure, the reader is referred to the web version of this article.)

simulated approximations of configurations A–D as well as bare and moderated variants of americium–beryllium (AmBe), plutonium–beryllium (PuBe), and americium–lithium (AmLi).

As shown in the summarized empirical results in Fig. 20, the **6C** spectrometer consistently outperforms the **4RP** spectrometer in positively identifying neutron sources in less time. In the case of the **6C** spectrometer (solid lines in Fig. 20), the experimental results may seem surprising upon initial inspection, as two of the source configurations with additional moderator/absorber (configurations B and C in Fig. 19, solid red and blue lines in Fig. 20 respectively) were positively identified in less time than the lightly moderated configuration with the NIST sphere alone (configuration A in Fig. 19, solid black line in Fig. 20). This result is informative in that it highlights the pragmatically significant relationship between the instrument's intrinsic efficiency and the correlation coefficient method of neutron source identification. In order to achieve a positive neutron source ID in the shortest amount of time with the correlation coefficient method, a high count rate is needed to provide sufficient counting statistical accuracy in the shortest amount of time. Since the **6C** spectrometer is most efficient to neutrons at the bottom end of the fast neutron energy range, the instrument achieved the highest count rate from the source configuration with an additional 1" of HDPE (higher amount of neutron moderation, configuration B), and identified this configuration in the shortest amount of time for all distances measured. The **6C** achieved the next highest count rate from the configuration with H_3BO_3 (boric acid) surrounding the NIST sphere (configuration C) and yielded the next best identification results. This relatively high count rate is due to the additional moderation via elastic scattering with hydrogen atoms in the boric acid. However, this effect is partially counteracted by moderately high energy neutron absorptions by ^{10}B atoms (also present in boric acid) at these energies, despite the reduced cross-section. Configuration D, with both 1 in. of HDPE and boric acid surrounding the NIST sphere, yielded the lowest count rate in the **6C** spectrometer. This relatively low count rate is due to the fact that many of the high energy neutrons exiting the NIST sphere are sufficiently moderated by the 1 in. of HDPE surrounding the sphere to have a high probability of subsequent absorption in the boric acid surrounding the HDPE. However, despite this heavy moderation and absorption, the **6C** instrument was still able to positively identify the neutron source in less than 90 s at a distance of 4.5 m. Although similar trends can be seen in the **4RP** spectrometer results, the aforementioned effects are skewed due to this spectrometer's greater sensitivity to environmental scattering effects. In other words, neutrons scattered off the ground are detected after entering the instrument from the bottom, decreasing the statistical predictability of the axial count distribution ($N_A(z)$ in Eq. 2) on which the correlation coefficient method of neutron source identification is based.

4. Conclusion

Four solid-state, moderating-type neutron spectrometers were designed, fabricated, and tested in an effort to improve on the neutron source detection and identification capabilities of long counters and Bonner-sphere-based instruments while making them portable. Through moderator geometry optimization, it was found that an instrument with a cylindrical moderator geometry can achieve a greater intrinsic neutron detection efficiency and greater energy sensitivity than an instrument with a rectangular prism geometry of the same weight. In studying the effects of individual MSND thermal neutron detection efficiency on overall instrument performance, it was shown that increasing the MSND thermal neutron detection efficiency above 22% provides diminishing returns to an instrument's intrinsic efficiency to bare ^{252}Cf. Through theoretical examination of the ratio between an instrument's outer moderator radius and outer detector radius, an outer detector radius of 3.8 cm and outer moderator radius of 7.8 cm (to reflect outbound neutrons) was found to be optimal for a cylindrical instrument of approximately 15 lb. After investigation of various moderator materials' effects on operational performance metrics, it was shown that increasing the hydrogen concentration of the moderator material drastically increases an instrument's intrinsic neutron detection efficiency and energy sensitivity. In this materials study, high density polyethylene was found to be more optimal for a wider range of applications than the other materials tested. Of the four fabricated spectrometers, the **5C** design exceeds the others in every category of operation, but is the most complex, the most costly to build, and the most physically cumbersome to operate. The **6C**, **4RP**, and **4C** designs were optimized and built to address the deficiencies of the **5C** design while simultaneously maximizing their individual operational performance, under increasingly restrictive cost and weight constraints, in order to mitigate the unavoidable tradeoffs associated with decreases in moderator volume and/or active detector area. These four instruments are the first representatives of a new class of hand-held, semiconductor-based, moderating-type neutron spectrometers of varying cost, weight, and design complexity, that provide a means to high intrinsic detection efficiency and neutron source identification through real-time energy-sensitive measurements of free neutron fields, ranging from thermal energies to the high end of the evaporation spectrum.

Acknowledgments

This work was funded by the Office of Naval Research, Award nos. N00014-11-1-0157 and N00014-13-1-0402, and by the Defense Threat Reduction Agency, Award no. HDTRA1-14-P-005. ANC wishes to thank Mark Strickman in performing the SWORD simulations.

Appendix A. Supplementary material

Supplementary data associated with this article can be found in the online version at 10.1016/j.nima.2015.08.077.

References

[1] Thomas M. Oakes, S.L. Bellinger, W.H. Miller, E.R. Myers, R.G. Fronk, B.W. Cooper, T.J. Sobering, P.R. Scott, P. Ugorowski, D.S. McGregor, J.K. Shultis, A.N. Caruso,

Nuclear Instruments and Methods in Physics Research Section A: Accelerators, Spectrometers, Detectors and Associated Equipment 719 (2013) 6.
[2] Richard L. Bramblett, R.I. Ewing, T.W. Bonner, Nuclear Instruments and Methods 9.1 (1960) 1.
[3] Walter J. McNeil, S.L. Bellinger, T.C. Unruh, C.M. Henderson, P. Ugorowski, B. Morris-Lee, R.D. Taylor, D.S. McGregor., Nuclear Instruments and Methods in Physics Research Section A: Accelerators, Spectrometers, Detectors and Associated Equipment 604 (1) (2009) 127.
[4] A.O. Hanson, J.L. McKibben, Physical Review 72 (8) (1947) 673.
[5] Y. Tanimura, J. Saegusa, M. Yoshida, Nuclear Instruments and Methods in Physics Research Section A: Accelerators, Spectrometers, Detectors and Associated Equipment 346 (1994) 273.
[6] Hiroki Tsuji, S. Maeda, H. Tomita, J. Kawarabayashi, T. Iguchi, T. Matsumoto, J.I. Hori, Progress in Nuclear Science and Technology 1 (2011) 316.
[7] Andrew C. Stephan, V. D. Jardret, Neutron Detector, United States Patent no. 7514,694, 2009.
[8] Anthony N. Caruso, Journal of Physics: Condensed Matter 443201 (2010) 22.
[9] IAEA, Compendium of Neutron Spectra and Detector Responses for Radiation Protection Purposes, Technical Reports Series no. 403, Supplement to Technical Reports Series no. 318, Vienna, 2001.
[10] Marcel Reginatto, P. Goldhagen, S. Neumann, Nuclear Instruments and Methods in Physics Research Section A: Accelerators, Spectrometers, Detectors and Associated Equipment 476 (1) (2002) 242.
[11] Marcel Reginatto, Radiation Measurements 45 (10) (2010) 1323.
[12] Karl Pearson, Proceedings of the Royal Society of London 58 (1895) 240.
[13] J.K. Shultis, D.S. McGregor, Nuclear Instruments and Methods in Physics Research A: Accelerators, Spectrometers, Detectors and Associated Equipment 606 (2009) 608.
[14] Steven L. Bellinger, R.G. Fronk, T.J. Sobering, D.S. McGregor, Applied Radiation and Isotopes 70 (7) (2012) 1121.
[15] Marcel Reginatto, Nuclear Instruments and Methods in Physics Research Section A: Accelerators, Spectrometers, Detectors and Associated Equipment 480 (2) (2002) 690.
[16] Brian W. Cooper, S.L. Bellinger, A.N. Caruso, R.G. Fronk, W.H. Miller, T.M. Oakes, J.K. Shultis, T.J. Sobering, D.S. McGregor, Neutron energy spectrum with microstructured semiconductor neutron detectors, in: Proceedings of the Nuclear Science Symposium and Medical Imaging Conference (NSS/MIC), IEEE, 2011, pp. 4783–4786.
[17] Mark J. Harrison, Q. Cherel, M. Monterial, Oak Ridge National Laboratory (ORNL), 2011.
[18] Mark J. Harrison, Q. Cherel, M. Monterial, Design of a moderated multidetector neutron spectrometer for optimal specificity, in: Proceedings of the Nuclear Science Symposium and Medical Imaging Conference (NSS/MIC), IEEE, 2011, pp. 4787–4794.
[19] Steven L. Bellinger, A.N. Caruso, B.W. Cooper, R.G. Fronk, C.B. Hoshor, D.S. McGregor, W.H. Miller, E.R. Myers, T.M. Oakes, B.J. Rogers, P.B. Ugorowski, J.K. Shultis, S.M. Young, Apparatuses and Methods for the Localization and Identification of Neutron Sources and/or Neutron Shielding Materials and Neutron Dose Equivalent, USPTO No. 9,081,100 issued 14 July, 2015.
[20] Paul Goldhagen, Nuclear Technology: Radiation, Measurements and General Instrumentation 175 (1) (2011) 81–88.
[21] Steven L. Bellinger, R.G. Fronk, W.J. McNeil, T.J. Sobering, D.S. McGregor, IEEE Transactions on Nuclear Science NS59 (1) (2012) 167.
[22] Simon R. Bolding, Design of a Neutron Spectrometer and Simulations of Neutron Multiplicity Experiments with Nuclear Data Perturbations (Master of Science thesis), Kansas State University, Manhattan, Kansas, 2013.
[23] Thomas M. Oakes, Modeling and Analysis of a Portable, Solid-State Neutron Detection System for Spectroscopic Applications (Doctor of Philosophy Dissertation), University of Missouri, Columbia, Missouri, 2012.